Chemical Science

ROYAL SOCIETY OF CHEMISTRY

EDGE ARTICLE

View Article Online
View Journal | View Issue

Cite this: *Chem. Sci.*, 2024, **15**, 3357

All publication charges for this article have been paid for by the Royal Society of Chemistry

Received 16th November 2023
Accepted 2nd January 2024

DOI: 10.1039/d3sc06155h

rsc.li/chemical-science

Stabilized four-electron aqueous zinc–iodine batteries by quaternary ammonium complexation†

Pengjie Jiang,‡ Qijun Du,‡ Chengjun Lei, Chen Xu, Tingting Liu, Xin He and Xiao Liang *

Four-electron aqueous zinc–iodine batteries (4eZIBs) leveraging the $I^-/I^0/I^+$ redox couple have garnered attention for their potential high voltage, capacity, and energy density. However, the electrophilic I^+ species is highly susceptible to hydrolysis due to the nucleophilic attack by water. Previous endeavors to develop 4eZIBs primarily relied on highly concentrated aqueous electrolytes to mitigate the hydrolysis issue, nonetheless, it introduced challenges associated with dissolution, high electrolyte viscosity, and sluggish electrode kinetics. In this work, we present a novel complexation strategy that capitalizes on quaternary ammonium salts to form solidified compounds with I^+ species, rendering them impervious to solubilization and hydrolysis in aqueous environments. The robust interaction in this complexation chemistry facilitates a highly reversible $I^-/I^0/I^+$ redox process, significantly improving reaction kinetics within a conventional $ZnSO_4$ aqueous electrolyte. The proposed 4eZIB exhibits a superior rate capability and an extended lifespan of up to 2000 cycles. This complexation chemistry offers a promising pathway for the development of advanced 4eZIBs.

Introduction

The development of four-electron aqueous zinc–iodine batteries (4eZIBs) with consecutive $I^-/I^0/I^+$ redox couples has sparked considerable interest in the realm of energy storage, driven by their impressive theoretical specific capacity, abundant resources, and environmental sustainability.[1–3] However, the widespread adoption of these batteries faces significant challenges that impact their stability and overall performance.[3–5] Among these challenges, the hydrolysis of positive valence I^+ species (such as ICl or ICl_2^-) in aqueous electrolytes stands out as a primary concern.[5–8] While the formation of ICl interhalogens during the electro-oxidation of iodine is thermodynamically favorable in the presence of nucleophiles like halides, it is highly susceptible to hydrolysis due to the nucleophilic attack by water's OH moieties.[9–11] This hydrolysis process results in low coulombic efficiency, voltage degradation, and poor cycling performance.

Previous attempts to address these issues in $I^-/I^0/I^+$ redox couples involved the use of super-concentrated aqueous electrolytes or non-aqueous electrolytes.[8,12–15] Nevertheless, the latter approach, while proficient at stabilizing the oxidized iodine species, has been plagued by complications related to the dissolution of active materials. This predicament arises from the high solubility of iodine and ICl interhalogens in organic solvents.[16–18] In contrast, the super-concentrated aqueous electrolyte approach we previously established, known as the 19–19–8 formula (specific molality of $ZnCl_2$, LiCl, and acetonitrile in water), has demonstrated notable success in mitigating the hydrolysis of I^+ species in an aqueous media. Such an electrolyte provides the requisite free chloride ions for the stabilization of I^+ species while simultaneously suppressing free water activity to participate in the hydrolysis. However, it introduced challenges associated with high electrolyte viscosity, which, in turn, hindered ion transport and led to sluggish electrode kinetics. To advance the development of 4eZIBs towards practicality, there is a compelling need to explore solutions that effectively suppress hydrolysis and dissolution, while simultaneously enhancing electrode redox kinetics in low-concentration aqueous electrolytes.

This study explores the application of quaternary ammonium salts to resolve these challenges in a dilute aqueous electrolyte composed of the commonly used $ZnSO_4$. Quaternary ammonium salts, known for their ability to form stable complexes with iodine species, hold the potential to significantly improve the stability and overall performance of the 4eZIB. In this work, we delve into the electrochemical behavior, complexation chemistry, and mechanisms governing the $I^-/I^0/I^+$ redox couple in zinc–iodine batteries, offering insights into the transformation of iodine states and the provision of a stable environment for I^+ within a dilute aqueous electrolyte. These findings pave the way for advancements in the design and

State Key Laboratory of Chem/Biosensing and Chemometrics, College of Chemistry and Chemical Engineering, Hunan University, Changsha, 410082, P. R. China. E-mail: xliang@hnu.edu.cn

† Electronic supplementary information (ESI) available. See DOI: https://doi.org/10.1039/d3sc06155h

‡ P. Jiang and Q. Du contributed equally to this work.

implementation of zinc–iodine batteries, with a focus on mitigating solubility and stability challenges, and thereby contributing to the development of more sustainable energy storage solutions.

Results and discussion

The complexation chemistry between ICl_2^- and quaternary ammonium cations

Previous research has established the possibility of quaternary ammonium cations forming complexes with polyhalides, including Br_3^-, ICl_2^-, and I_3^-.[19–22] The complexation approaches have been validated in halogen batteries with the I^-/I^0 and Br^-/Br^0 redox couples.[23–25] In this work, the complexation chemistry between ICl_2^- and quaternary ammonium cations was investigated to elucidate the stability of I^+ in aqueous media. Various quaternary ammonium cations with differing chain lengths as the complexing agents were selected. The corresponding quaternary ammonium dichloroiodates ($QICl_2$ compounds) were synthesized by simple redox reactions (see the Experimental section for details), with their molecular structures shown in Fig. S1.† Fig. S2a† visually illustrates the $QICl_2$ compounds, which are in the powder form at room temperature.

Raman spectroscopy was employed to characterize the as-prepared precipitates. Fig. 1a demonstrates that the symmetric stretching of the I–Cl band occurs around 270 cm^{-1}, while the asymmetric stretching occurs around 250 cm^{-1}.[26–30] There is an observable blue-shift and subsequent red-shift of the specific Raman signal corresponding to the I–Cl bond with increasing chain lengths of the quaternary ammonium cations, indicating a varying intensity of the complexation effect. Among all $QICl_2$ compounds, Pr_4NICl_2 exhibits the most pronounced complexation effect as revealed by the Raman spectrum (Fig. 1a), detailed Raman results for $QICl_2$ compounds within a broader measuring range can be found in Fig. S3.† This is consistent with the binding energies among all $QICl_2$ compounds in a vacuum environment, as determined by the first principles calculations based on density functional theory (DFT) (Fig. 1b). However, the complexation energy of quaternary ammonium cations with ICl_2^- would be influenced if water was considered in the simulation system (Fig. S4†). The results indicate that, in the presence of water, $Hexy_4NICl_2$ exhibits the highest binding energy, followed by Am_4NICl_2 and Pr_4NICl_2. We also assessed the complexation effect of $QICl_2$ compounds through observing their status in distilled water visually. Me_4NICl_2 and Et_4NICl_2 are soluble in distilled water and exhibit the typical ICl_2^- Raman signal right after the preparation of the solution (Fig. 1c and S5†).

In contrast, the remaining $QICl_2$ compounds were insoluble in distilled water, forming a separated phase. This observation can be elucidated by the similarity–intermiscibility theory, suggesting that the $QICl_2$ compounds become progressively more lipophilic and hydrophobic with increasing chain length.[31] Even after 6 months immersion, these initially insoluble $QICl_2$ compounds remain as a separated phase in water (Fig. S2b†), albeit with some degree of aggregation in shape. This is consistent with the calculated binding energy results of these $QICl_2$ compounds (Fig. S4†), which shows that the long-term stability of these materials in water mainly depends on the strength of their complexation interaction. On the other hand, the corresponding quaternary ammonium chloride (QCl)

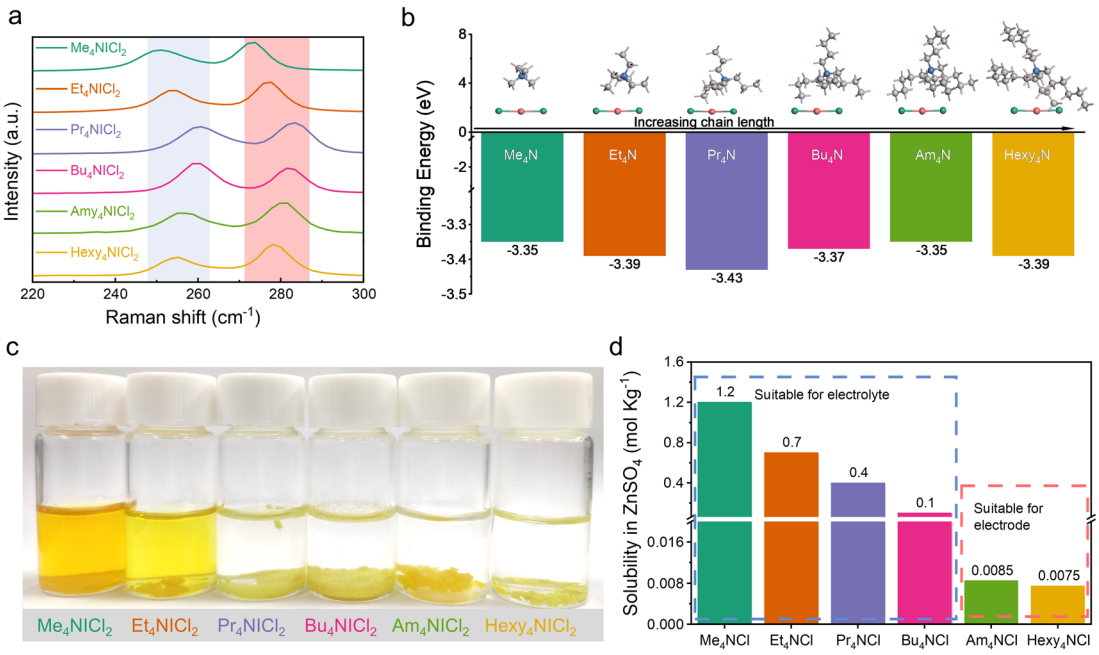

Fig. 1 Complexation of quaternary ammonium cations with ICl_2^-. (a) Raman spectra of the $QICl_2$ compounds. (b) The calculated binding energy of quaternary ammonium cations with ICl_2^- in a vacuum environment. (c) Digital photo of $QICl_2$ compounds in H_2O for a week. (d) The solubility of $QICl_2$ compounds in $ZnSO_4$ electrolyte.

has distinct solubility in water and electrolytes (Fig. 1d and ESI Table 1†), which could be attributed to their alkyl chain-length dependent hydrophobicity.

The solubility tests of the $QICl_2$ compounds were also conducted in commonly used $ZnSO_4$ based aqueous electrolytes. Similar to their behavior in distilled water, all $QICl_2$ compounds, except for Me_4NICl_2 and Et_4NICl_2, are insoluble in electrolytes of 1 m $ZnSO_4$ + 1 m $ZnCl_2$ (Fig. S2c†) and 3 m $ZnSO_4$ + 1 m $ZnCl_2$ (Fig. S2d†). Notably, for Me_4NICl_2 and Et_4NICl_2, their solubility in the electrolyte was lower compared to that in water, as the color of the electrolyte solution was much clearer. These results indicate that electrolyte solutions also offer a more stable environment for $QICl_2$ compounds than distilled water.

Furthermore, the stability of $QICl_2$ compounds was evaluated using thermogravimetry analysis (Fig. S6a and b†), verifying the strong complexation from a thermal decomposition perspective. The melting points of all $QICl_2$ compounds are above 100 °C, which are higher than that of free ICl (27.2 °C in the α-form or 13.9 °C in the β-form),[32] indicating their exceptional thermal stability. Moreover, $QICl_2$ compounds remain in the solid state at room temperature, even after a long-term storage in air (Fig. S2a†), unlike ICl, which is a volatile liquid, and prone to hydrolysis.[33]

$QICl_2$ compounds with the strong complexation exhibit superior chemical stability in mitigating hydrolysis compared to the free ICl without complexation (Fig. 2a). Equimolar amounts of these compounds were dispersed/dissolved in water (~0.1 M). The solution/suspensions after relaxation were diluted with acetonitrile before the UV-vis spectroscopy test. Free ICl is highly susceptible to hydrolysis due to the nucleophilic attack by water.[9–11] As depicted in Fig. S7,† the intensity of the UV absorption peak associated with free ICl (335 nm) quickly diminished when subjected to H_2O attack, while the UV absorption peak ascribed to I_2 (450 nm) increased. This shift indicates the hydrolysis of iodine monochloride, resulting in the formation of I_2.[34] $QICl_2$ compounds exhibited varying degrees of attenuation in the intensity of their specific UV absorption peak at 335 nm in response to water attack (Fig. 2b and S7†), with Pr_4NICl_2 showing the slowest rate of hydrolysis by normalization of their UV adsorption intensities (Fig. 2c).

The hydrolysis process was further calculated (Fig. 2d), confirming that Pr_4NICl_2 possesses the highest hydrolysis energy barrier among various $QICl_2$ compounds. Detailed representations of the initial state, transition state, and final state of various $QICl_2$ compounds during hydrolysis can be found in Fig. S9–S14.† These results collectively suggest that the dissolution and hydrolysis of I^+ species in an aqueous electrolyte could be effectively mitigated by the complexation strategy.

Validating the complexation chemistry through electrolyte additives

To assess the stability of the I^0/I^+ redox couple employing a quaternary ammonium salt complexation approach, we introduced Me_4NCl, Et_4NCl, Pr_4NCl and Bu_4NCl into a conventional $ZnSO_4$ electrolyte for evaluation. These cells were

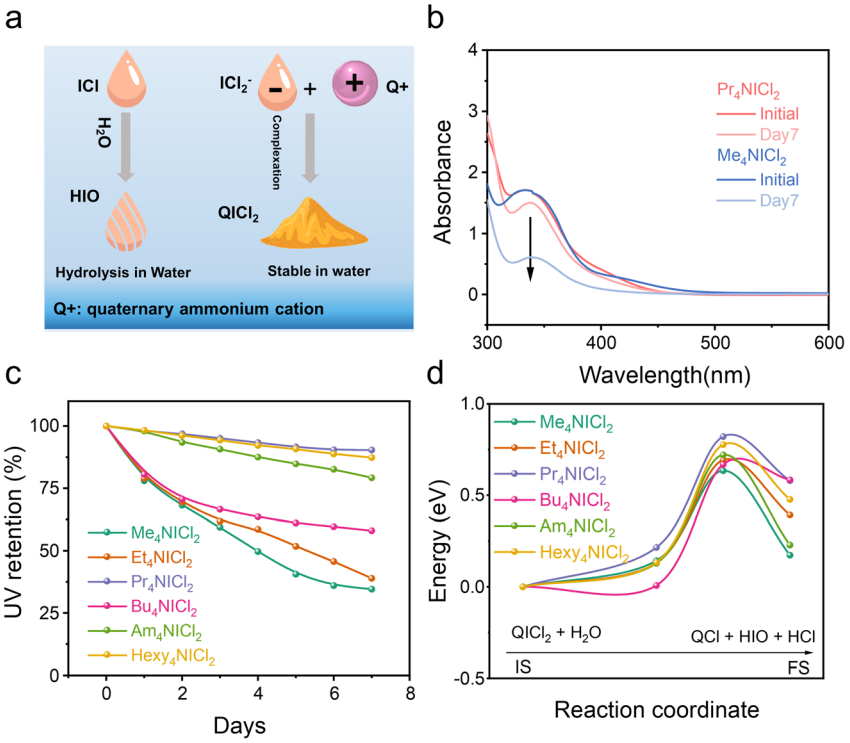

Fig. 2 Stability of $QICl_2$ compounds in aqueous media. (a) Schematic diagram of the complexation and stability of quaternary ammonium salts with ICl^- in aqueous media. (b) Typical UV-vis spectra of $QICl_2$ compounds before and after H_2O attack. (c) Retention of $QICl_2$ compounds by UV-vis spectral analysis. (d) Calculated energy barrier for the hydrolysis process of $QICl_2$ compounds.

composed of a PAC/I_2 cathode and a zinc foil anode. It is important to note that other quaternary ammonium salts with longer chain lengths cannot be used as electrolyte additives due to their limited solubility in the $ZnSO_4$ electrolyte (Fig. 1d and ESI Table 1†). These will be studied as the cathode in the following sections.

Focusing on the I^0/I^+ redox couple within the voltage range of 1.25–1.8 V *versus* Zn/Zn^{2+}, we observed that batteries supplemented with KCl and Me_4NCl additive exhibited an inclined charge/discharge profile with a short platform (Fig. S15a†). In contrast, the batteries incorporating Et_4NCl, Pr_4NCl, and Bu_4NCl displayed a flat charge/discharge profile, indicative of a more reversible redox process. Furthermore, Pr_4NCl exhibited the highest coulombic efficiency, as shown in Fig. S15b,† suggesting that the I^+ hydrolysis during the charge/discharge process is effectively mitigated. The stability of I^+ was quantified by measuring the retained capacity of the I^0/I^+ couple (discharged to 1.25 V) after extended storage using a fully charged Zn–I_2 cell (charged to 1.8 V) at open-circuit voltage. As illustrated in Fig. S15c,† following a 24 hour resting period, the battery with Pr_4NCl as an additive maintained a discharge plateau, while batteries with other additives displayed a declining discharge profile.

We also investigated the stability of the battery over an extended resting time for the $I^-/I^0/I^+$ multiple electron transformation process within the voltage range of 0.6–1.8 V. As anticipated, the battery supplemented with Pr_4NCl exhibited both the highest coulombic efficiency and the most distinct I^+ discharge platform, as depicted in Fig. 3a and S16a.† These results strongly support the complexation strategy to improve I^+ stability in a dilute aqueous electrolyte environment, especially when using Pr_4NCl as an additive. In the context of the 4eZIB employing quaternary ammonium chloride electrolyte additives, all the batteries exhibit two pairs of charge/discharge plateaus (Fig. 3b). Specifically, Pr_4NCl displayed the flattest I^0/I^+ discharge platform and the lowest capacity degradation rate (Fig. S16b†). The Pr_4NCl concentration was further investigated (Fig. S16c†). The discharge plateaus at 1.6 V (I^0/I^+) are elongated rationally with the increase of the Pr_4NCl additive in the electrolyte. However, when an excessive additive was introduced (0.2 m Pr_4NCl in the electrolyte), an excess of Pr_4NICl_2 passivation layer on the electrode might be formed, resulting in significant polarization during charge/discharge. Galvanostatic intermittent titration technique (GITT) profiles were collected to investigate the kinetic mechanism (Fig. S17†). The calculated diffusion coefficient indicates a substantial drop by 2 orders of magnitude at the high plateau, which can be attributed to the formation of the Pr_4NICl_2 phase that is hydrophobic in aqueous media thus impeding ion migration.

We conducted *ex situ* UV-vis absorption spectroscopy and *in situ* Raman spectroscopy focusing on the electrode to elucidate the electrode composition. Fig. 3c shows the *ex situ* UV-vis spectrum during the charge/discharge process in a 3 m $ZnSO_4$ + 0.1 m Pr_4NCl electrolyte. During the charging process, the detected iodine species undergo a transformation from I^- (244 nm)[35] into I_3^- (295 nm and 365 nm),[36] I_2Cl^- (264 nm),[37] ICl_2^-

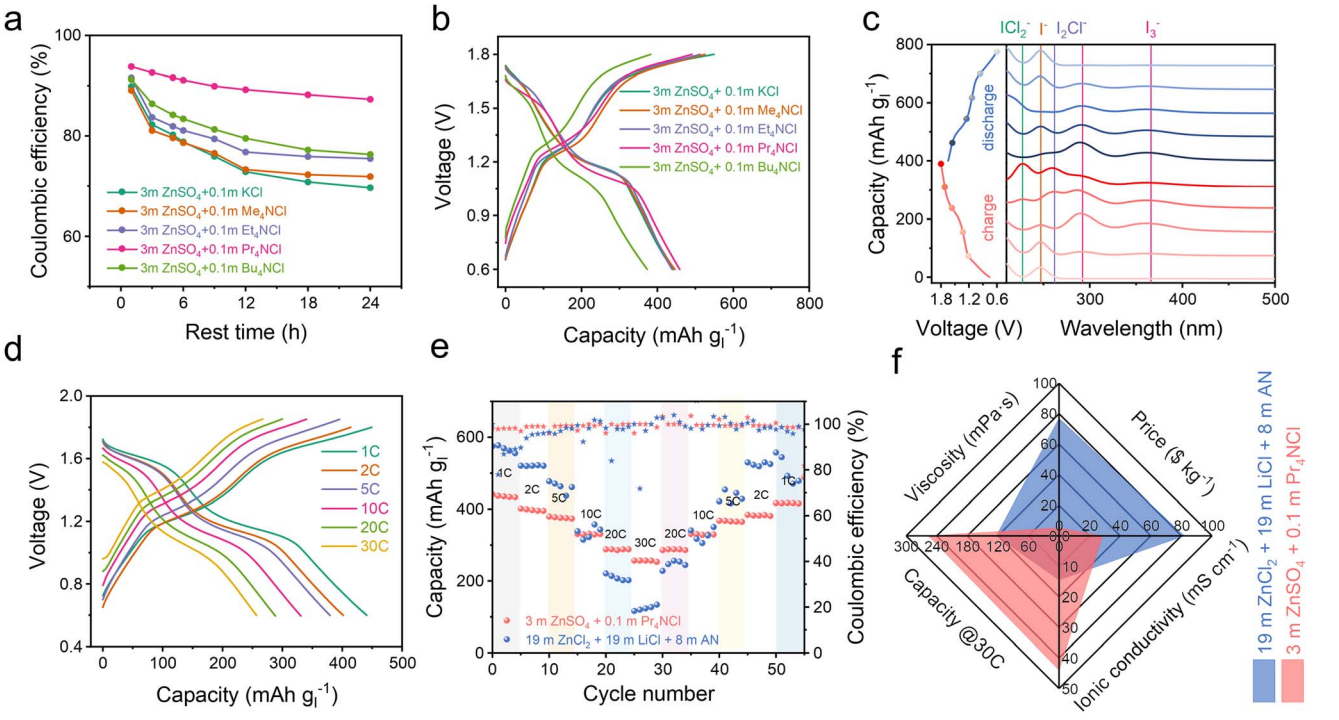

Fig. 3 Quaternary ammonium chlorides as electrolyte additives. (a) Self-discharge of the 4eZIBs after various resting periods in different electrolytes. (b) Voltage profiles of 4eZIBs within the voltage range of 0.6–1.8 V. (c) *Ex situ* UV-vis absorption spectrum of the 4eZIBs with the 3 m $ZnSO_4$ + 0.1 m Pr_4NCl electrolyte. (d) Voltage profiles of 4eZIBs with different rates, the electrolyte is 3 m $ZnSO_4$ + 0.1 m Pr_4NCl. (e) The rate capability of the 4eZIBs. (f) The characteristics of different electrolytes.

(230 nm).[37,38] Notably, 230 nm (C-/D-absorption band) and 335 nm (A-/B-absorption band) are both the characteristic absorption bands of ICl_2^-, which are concentration sensitive due to the UV absorption efficiency.[37,39] The characteristic Raman signal around 167 cm^{-1} exhibits changes during charge/discharge to 1.6 V/1.4 V (Fig. S18†), corresponding to the bending vibration for ICl_2^-.[27] These results are similar to our previous report,[8] indicating an $I^-/I^0/I^+$ redox process, however, this is achieved in a dilute aqueous electrolyte enabled by the complexation chemistry.

After 1000 cycles, the battery still exhibits distinct charge/discharge plateaus (Fig. S19a†), revealing an unchanged primary electrochemical reaction process (I^-/I^0 and I^0/I^+). Impressively, the battery employing the 3 m $ZnSO_4$ + 0.1 m Pr_4NCl electrolyte achieves a capacity of 442 mA h g^{-1} at 1C, and 252 mA h g^{-1} at 30C based on iodine mass (Fig. 3d). As demonstrated in Fig. 3e, the zinc–iodine battery shows an excellent rate performance for the 3 m $ZnSO_4$ + 0.1 m Pr_4NCl than in a conventional high concentration 19–19–8 electrolyte (19 m $ZnCl_2$ + 19 m LiCl + 8 m AN in water). These could be ascribed to the low viscosity (5.3 mPa s) and high ionic conductivity (44 mS cm^{-1}) of the 3 m $ZnSO_4$ + 0.1 m Pr_4NCl electrolyte, as shown in Fig. 3f. Furthermore, the quite dilute electrolyte also proves to be more cost-effective with 28.4 $ per kg than the concentrated electrolyte (81.9 $ per kg). The zinc–iodine battery with the 3 m $ZnSO_4$ + 0.1 m Pr_4NCl electrolyte demonstrates exceptional longevity, sustaining over 1100 cycles at 5C with 74% capacity retention (Fig. S19b†). The reliability of the complexation strategy was also accessed at a high current density of 4420 mA g^{-1} (10C), where it underwent more than 5000 cycles with minor degradation (Fig. S19c†).

Application of the complexation chemistry in an electrode

While the use of quaternary ammonium salts as electrolytes has demonstrated success, the solubility of these salts in electrolytes (*i.e.* 0.4 m for Pr_4NCl in 3 m $ZnSO_4$ electrolyte), along with the required volume of the electrolytes for a high areal capacity, imposes constraints on the energy density of 4eZIBs. In response to this challenge, we propose employing $QICl_2$ compounds directly as cathodes. In these cases, the insoluble but strong complexing Hexy- and Amy-quaternary ammonium salts can be utilized, while the electrolyte is composed of 3 m $ZnSO_4$ + 1 m $ZnCl_2$. Note that the specific capacity was based on the mass fraction of iodine, if not specified, so as to facilitate comparison.

As shown in Fig. 4a and S20,† the Me_4NICl_2 and Et_4NICl_2 cathodes in the 3 m $ZnSO_4$ + 1 m $ZnCl_2$ electrolyte exhibited fast capacity decay due to their solubility in the electrolyte as discussed in Fig. 1c. Conversely, the $Hexy_4NICl_2$ cathode showed minimal capacity fade and a consistent charge/discharge profile for long-term cycling, which is correlated with their strong complexation ability to ICl_2^- anion. An intriguing observation is the shift in the equilibrium potential of quaternary ammonium dichloroiodates from ~1.7 V for Me_4NICl_2 and Et_4NICl_2 to ~1.6 V for others. This shift can be attributed to the change of ICl_2^- from a partially dissociated/hydrolyzed environment to a tightly associated hydrophobic environment in aqueous

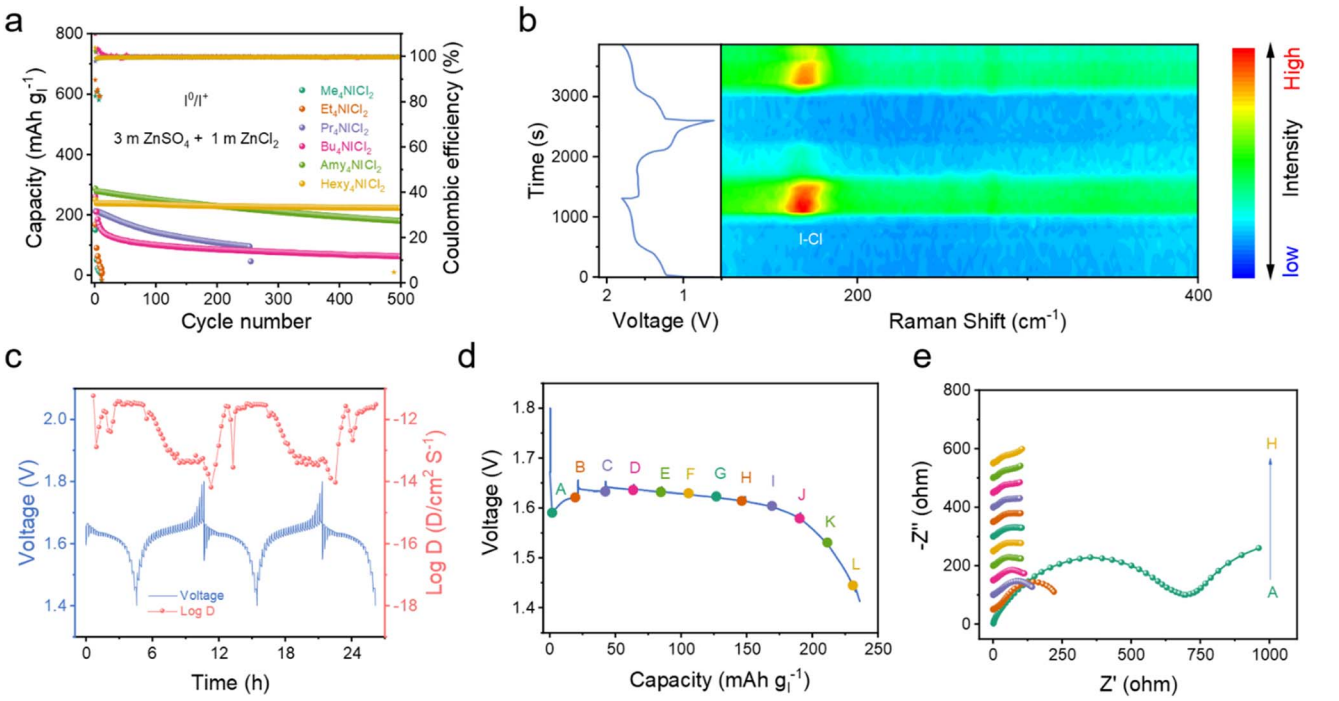

Fig. 4 Electrochemical mechanism of the 4eZIBs using the $QICl_2$ cathode. (a) Cycling performance of various $QICl_2$ compounds. (b) *In situ* Raman spectrum of $Hexy_4NICl_2$ during charge/discharge. (c) The GITT profile and corresponding diffusion coefficient of the $Hexy_4NICl_2$ electrode. (d) The voltage profile of the $Hexy_4NICl_2$ electrode and (e), the corresponding EIS spectrum at different depths of discharge. The electrolytes were 3 m $ZnSO_4$ + 1 m $ZnCl_2$.

electrolytes. When using an electrolyte comprising 1 m $ZnSO_4$ + 1 m $ZnCl_2$, the $Hexy_4NICl_2$ cathode showed robust performance with negligible capacity degradation, while Amy_4NICl_2 exhibited a relatively fast decay (Fig. S21†). These indicate that, in addition to the complexation chemistry, the kosmotropic $ZnSO_4$ electrolyte with its strong salting-out effect due to the intrinsic structured water formation ability, also plays a pivotal role in suppressing the dissolution/hydrolysis of the chaotropic quaternary ammonium dichloroiodates.[40,41]

Real-time monitoring of iodine species on the electrode by *in situ* Raman spectroscopy captured the typical Raman signal around 167 cm^{-1} (Fig. 4b), which either rose or disappeared during the charge/discharge process to 1.6 V/1.4 V, corresponding to the bending vibration (ν_2) of the I–Cl band.[29,30] Besides, the weak signal of the symmetric stretching and asymmetric stretching of the I–Cl band was also found when charged to 1.8 V (Fig. S22†). These relatively weaker signals compared to those of the synthesized $Hexy_4NICl_2$ might be attributed to the decreased crystallinity of the material formed by the electrochemical process.[26,42] These are in accordance with the redox process when using the quaternary ammonium salt as the electrolyte additive. The diffusion coefficient of the $Hexy_4NICl_2$ electrode reveals a reduction of nearly one order of magnitude at the beginning of the discharge process (Fig. 4c). This substantial decrease is likely attributed to the necessity of chemical bond deformation for the reduction/decomposition of $Hexy_4NICl_2$. The charge transfer resistance of the $Hexy_4NICl_2$ electrode at the beginning of the discharge process (point A) is the highest, further aligning with these observations (Fig. 4d and e). Additionally, Fig. S23† demonstrates that when the battery operates at 60 °C, the voltage drop during the initial discharge process is notably smaller compared to that at room temperature. This can be attributed to the improved reaction kinetics by the elevated temperature that facilitates the breaking of chemical interaction within $Hexy_4NICl_2$. However, it is important to note that the high temperature also increases the solubility of $Hexy_4NICl_2$, diminishing its stability in the electrolyte and resulting in a relatively low coulombic efficiency (about 88% at 60 °C).

By employing $Hexy_4NICl_2$ as the cathode, the Zn–I_2 battery based on the I^0/I^+ couple showed nearly consistent charge and discharge curves throughout 500 cycles (Fig. 5a), and 250 mA h g^{-1} at 1C. It should be noted that Super P contributes a small fraction of capacity in the operational voltage window (Fig. S24†). This Zn–I_2 battery based on the I^0/I^+ couple also showed a remarkable rate performance of 120 mA h g^{-1} at 100C (Fig. 5b) and sustained long-term cycle performance over 2000 cycles with an 88% capacity retention at 5C (Fig. 5c). For comprehensively understanding the role of the electrolyte in this battery system, we examined an electrolyte containing only $ZnSO_4$ (Fig. S25†). An electrolyte composed solely of $ZnSO_4$ resulted in rapid fading and pronounced polarization, highlighting that an extra Cl^- carrier in the electrolyte is also essential to accomplish the multi-electron conversion.

In the context of the $I^-/I^0/I^+$ redox couple within the $Hexy_4NICl_2$ cathode, the 4eZIB has two redox couples around 1.3 V and 1.6 V (Fig. 5d). The fitted *b* values of the four redox peaks are 0.664, 0.644, 0.519, and 0.517 respectively (Fig. S26†), indicating that the energy storage process is governed by a combination of

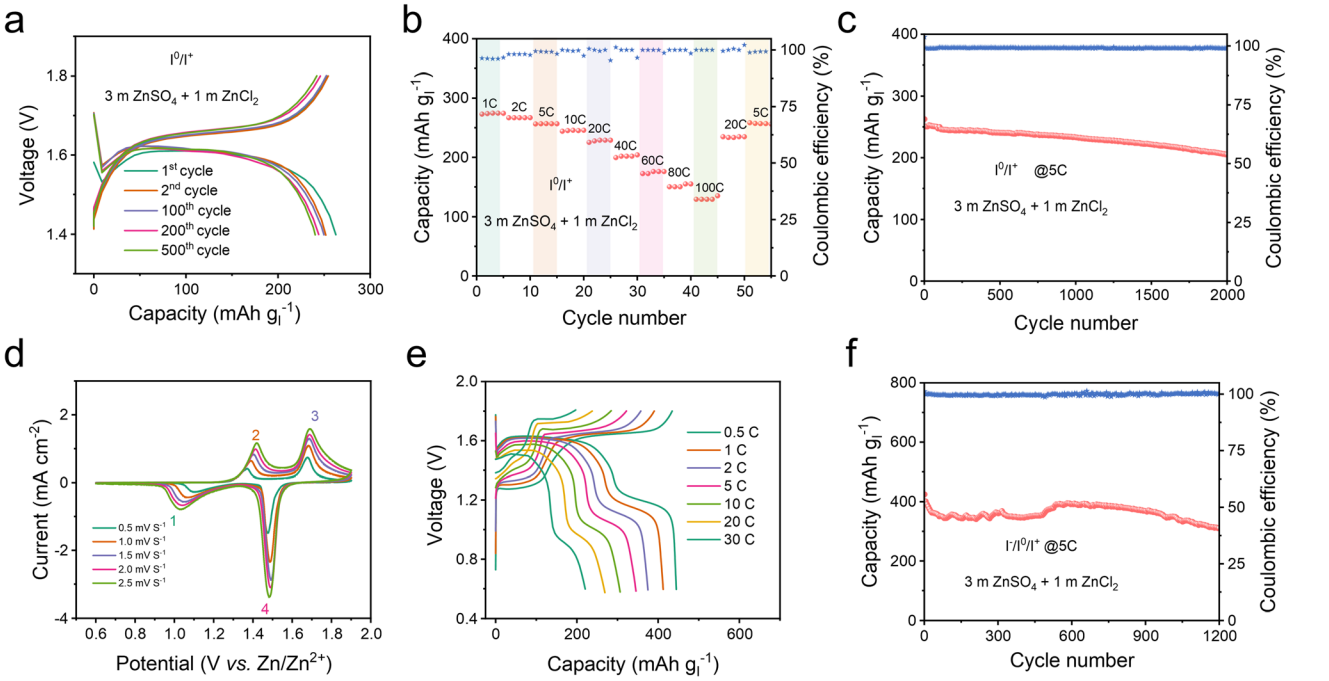

Fig. 5 Cycling performance of the 4eZIBs with the $Hexy_4NICl_2$ cathode. (a) Voltage profile, (b) rate behavior and (c) long term battery performance of $Hexy_4NICl_2$ within the voltage range of 1.4–1.8 V. (d) CV curves of $Hexy_4NICl_2$ at sweep rates from 0.5 to 2.5 mV s^{-1}. (e) Voltage profiles at various rates and (f) long term cycling performance of 4eZIBs within the voltage range of 0.6–1.8 V. The electrolyte was 3 m $ZnSO_4$ + 1 m $ZnCl_2$.

both the diffusion process and the pseudocapacitive process. The proposed 4eZIB exhibits a self-discharging rate of only 2.5% after charging to 1.8 V with a 5 hour rest period (Fig. S27†). This 4eZIB demonstrates two well-defined charge/discharge plateaus, even at a high rate of 30C, with a discharge capacity of about 445 mA h g^{-1} (or 118 mA h g^{-1} based on $Hexy_4NI$ mass) at 0.5C and 200 mA h g^{-1} (or 52 mA h g^{-1} base on $Hexy_4NI$ mass) at 30C (Fig. 5e and S28†). Additionally, the 4eZIB with the $Hexy_4NICl_2$ cathode can sustain operation at 5C (2110 mA h g^{-1}) for 1200 cycles while retaining 75% capacity (Fig. 5f and S29†).

We noticed that a trace of the quaternary ammonium salt in the electrolyte could also regulate the zinc anode electroplating process. In the blank electrolyte, the zinc anode exhibited an uneven deposition morphology (Fig. S30a†), which gave rise to a pronounced dendrite formation and a reduced lifespan of the battery. In contrast, the introduction of the $Hexy_4NCl$ additive (5 mmol kg^{-1}, close to its saturation) led to a dense plating of zinc under the same conditions (Fig. S30b†). In Zn||Ti asymmetric cells, the high surface area dendrites induced severe side reactions with the electrolyte, resulting in a low coulombic efficiency in the blank $ZnSO_4$ electrolyte (Fig. S30c†). In comparison, the Zn||Ti cells achieved an improved coulombic efficiency of 99.2% in the 5 mmol $Hexy_4NCl$ electrolyte. Moreover, repeated plating/stripping tests in Zn||Zn symmetric cells demonstrated the robustness of the zinc anode in the presence of the $Hexy_4NCl$ additive (Fig. S30d†).

Conclusions

In summary, this study focused on enhancing the stability and performance of 4eZIBs in the commonly used $ZnSO_4$ electrolyte through the utilization of symmetric quaternary ammonium salts with distinct chain lengths. These salts provide substantial complexation ability to I^+ species, which mitigated its hydrolysis/dissolution thus the electrochemical performance was improved. This study not only delved into the complexation chemistry but also elucidated the underlying mechanisms governing the $I^-/I^0/I^+$ redox couple, shedding light on the transformation of iodine states. Particularly, $Hexy_4NICl_2$ demonstrated excellent stability in aqueous media and served as an effective cathode, leading to superior rate capability and an extended lifespan of 4eZIB. These findings offer promising prospects for the practical application of 4eZIBs, addressing the solubility and stability concerns and providing a sustainable solution for energy storage systems. While we note that the symmetric quaternary ammonium cations take up a large amount of mass in comparison to iodine, further optimization of the ammonium salts with asymmetric structures or smaller molecular weights is necessary, which are currently being explored in our laboratory. Additionally, the formation of a stable hydrophobic $QICl_2$ layer on the iodine electrode might also prevent the hydrolysis of internally oxidized I^+ at a high iodine content.

Data availability

The data supporting this article have been uploaded as part of the ESI.† Additional data is available from the authors on reasonable request.

Author contributions

P. Jiang, Q. Du: electrochemical experiments and material synthesis; C. Lei: theoretical discussions; C. Xu, T. Liu: instrumental characterization; X. He: commentary or revision of the manuscript; X. Liang: proposed, designed and organized the work and wrote the manuscript; all the authors participated in the discussions and preparation of the manuscript.

Conflicts of interest

There are no conflicts to declare.

Acknowledgements

This work is supported by the National Key Research and Development Program of China (2019YFA0210600 and 2022YFB3807700) and National Natural Science Foundation of China (51972107 and 22309048).

Notes and references

1 F. Zhang, Q. Wang and Y. Tang, *Matter*, 2021, **4**, 2637–2639.
2 Y. Yang, S. Liang and J. Zhou, *Curr. Opin. Electrochem.*, 2021, **30**, 100761.
3 D. Lin and Y. Li, *Adv. Mater.*, 2022, 2108856.
4 X. Li, M. Li, Z. Huang, G. Liang, Z. Chen, Q. Yang, Q. Huang and C. Zhi, *Energy Environ. Sci.*, 2021, **14**, 407–413.
5 Z. Zhang, Y. Zhu, M. Yu, Y. Jiao and Y. Huang, *Nat. Commun.*, 2022, **13**, 1–11.
6 L. Yan, S. Zhang, Q. Kang, X. Meng, Z. Li, T. Liu, T. Ma and Z. Lin, *Energy Storage Mater.*, 2023, **54**, 339–365.
7 Y. Yang, S. Liang, B. Lu and J. Zhou, *Energy Environ. Sci.*, 2022, **15**, 1192–1200.
8 Y. Zou, T. Liu, Q. Du, Y. Li, H. Yi, X. Zhou, Z. Li, L. Gao, L. Zhang and X. Liang, *Nat. Commun.*, 2021, **12**, 170.
9 Q. Guo, K.-I. Kim, S. Li, A. M. Scida, P. Yu, S. K. Sandstrom, L. Zhang, S. Sun, H. Jiang, Q. Ni, D. Yu, M. M. Lerner, H. Xia and X. Ji, *ACS Energy Lett.*, 2021, 459–467.
10 Z. Xue, Z. Gao and X. Zhao, *Energy Environ. Mater.*, 2022, **5**, 1155–1179.
11 F. A. Philbrick, *J. Am. Chem. Soc.*, 1934, **56**, 1257–1259.
12 S. Lv, T. Fang, Z. Ding, Y. Wang, H. Jiang, C. Wei, D. Zhou, X. Tang and X. Liu, *ACS Nano*, 2022, **16**, 20389–20399.
13 J. Xu, T. P. Pollard, C. Yang, N. K. Dandu, S. Tan, J. Zhou, J. Wang, X. He, X. Zhang, A.-M. Li, E. Hu, X.-Q. Yang, A. Ngo, O. Borodin and C. Wang, *Joule*, 2023, **7**, 83–94.
14 X. Li, S. Wang, D. Zhang, P. Li, Z. Chen, A. Chen, Z. Huang, G. Liang, A. L. Rogach and C. Zhi, *Adv. Mater.*, 2023, 2304557.
15 X. Li, Y. Wang, Z. Chen, P. Li, G. Liang, Z. Huang, Q. Yang, A. Chen, H. Cui, B. Dong, H. He and C. Zhi, *Angew. Chem., Int. Ed.*, 2022, **61**, e202113576.
16 J. Ma, M. Liu, Y. He and J. Zhang, *Angew. Chem., Int. Ed.*, 2021, **60**, 12636–12647.
17 J. J. Hong, L. Zhu, C. Chen, L. Tang, H. Jiang, B. Jin, T. C. Gallagher, Q. Guo, C. Fang and X. Ji, *Angew. Chem., Int. Ed.*, 2019, **58**, 15910–15915.

18 F. Ascoli and F. M. Kahan, *J. Biol. Chem.*, 1966, **241**, 428–431.
19 S. Kajigaeshi, M. Moriwaki, S. Fujisaki, T. Kakinami and T. Okamoto, *Bull. Chem. Soc. Jpn.*, 1990, **63**, 3033–3035.
20 J. J. Novoa, F. Mota and S. Alvarez, *J. Phys. Chem.*, 1988, **92**, 6561–6566.
21 E. H. Wiebenga, E. E. Havinga and K. H. Boswijk, in *Advances in Inorganic Chemistry and Radiochemistry*, ed. H. J. Emeleus and A. G. Sharpe, Academic Press, 1961, vol. 3, pp. 133–169.
22 S. J. Yoo, B. Evanko, X. Wang, M. Romelczyk, A. Taylor, X. Ji, S. W. Boettcher and G. D. Stucky, *J. Am. Chem. Soc.*, 2017, **139**, 9985–9993.
23 L. Gao, Z. Li, Y. Zou, S. Yin, P. Peng, Y. Shao and X. Liang, *iScience*, 2020, **23**, 101348.
24 M. Wang, T. Li, Y. Yin, J. Yan, H. Zhang and X. Li, *Adv. Energy Mater.*, 2022, **12**, 2200728.
25 P. Li, X. Li, Y. Guo, C. Li, Y. Hou, H. Cui, R. Zhang, Z. Huang, Y. Zhao, Q. Li, B. Dong and C. Zhi, *Adv. Energy Mater.*, 2022, **12**, 2103648.
26 A. G. Maki and R. Forneris, *Spectrochim. Acta, Part A*, 1967, **23**, 867–880.
27 W. B. Person, G. R. Anderson, J. N. Fordemwalt, H. Stammreich and R. Forneris, *J. Chem. Phys.*, 1961, **35**, 908–914.
28 T. J. Emge, H. H. Wang, P. C. W. Leung, P. R. Rust, J. D. Cook, P. L. Jackson, K. D. Carlson, J. M. Williams, M. H. Whangbo, *et al.*, *J. Am. Chem. Soc.*, 1986, **108**, 695–702.
29 M. S. Abdelbassit, O. J. Curnow, M. K. Dixon and M. R. Waterland, *Chem.–Eur. J.*, 2019, **25**, 11650–11658.
30 W. Gabes and H. Gerding, *J. Mol. Struct.*, 1972, **14**, 267–279.
31 K. J. Shah, M. K. Mishra, A. D. Shukla, T. Imae and D. O. Shah, *J. Colloid Interface Sci.*, 2013, **407**, 493–499.
32 D. P. Day, N. I. Alsenani and A. A. Alsimaree, *Eur. J. Org Chem.*, 2021, **2021**, 4299–4307.
33 D. Janas, A. P. Herman, S. Boncel and K. K. K. Koziol, *Carbon*, 2014, **73**, 225–233.
34 Y. L. Wang, J. C. Nagy and D. W. Margerum, *J. Am. Chem. Soc.*, 1989, **111**, 7838–7844.
35 J. Jortner and A. Treinin, *Trans. Faraday Soc.*, 1962, **58**, 1503–1510.
36 W. Gabes and D. J. Stufkens, *Spectrochim. Acta, Part A*, 1974, **30**, 1835–1841.
37 S. Schott, L. Ress, J. Hrušák, P. Nuernberger and T. Brixner, *Phys. Chem. Chem. Phys.*, 2016, **18**, 33287–33302.
38 A. I. Popov and R. F. Swensen, *J. Am. Chem. Soc.*, 1955, **77**, 3724–3726.
39 W. Gabes and D. J. Stufkens, *Spectrochim. Acta, Part A*, 1974, **30**, 1835–1841.
40 N. J. Bridges, K. E. Gutowski and R. D. Rogers, *Green Chem.*, 2007, **9**, 177–183.
41 W.-Y. Kim, H.-I. Kim, K. M. Lee, E. Shin, X. Liu, H. Moon, H. Adenusi, S. Passerini, S. K. Kwak and S.-Y. Lee, *Energy Environ. Sci.*, 2022, **15**, 5217–5228.
42 R. S. Halford, *J. Chem. Phys.*, 1946, **14**, 8–15.